Voltage-Oriented Input–Output Linearization Controller as Maximum Power Point Tracking Technique for Photovoltaic Systems

Diego R. Espinoza-Trejo, *Associate Member, IEEE*, Ernesto Bárcenas-Bárcenas, *Member, IEEE*, Daniel U. Campos-Delgado, *Senior Member, IEEE*, and Cristian H. De Angelo, *Senior Member, IEEE*

***Abstract*—This paper presents a robust input–output linearization controller as maximum power point tracking (MPPT) technique in a photovoltaic (PV) buck dc–dc converter with applications to dc microgrids, solar vehicles, or stand-alone systems. Due to the control structure proposed in this paper, the MPPT control system is able to track very fast irradiance changes. Meanwhile, the internal stability of the overall closed-loop system is guaranteed for different load scenarios. A sector condition is only required for the load current, which is satisfied for most of the current PV applications. In turn, this condition implies the robustness against oscillations in the dc bus voltage. Finally, the MPPT control system is validated through experimental results, where the closed-loop performance is evaluated under abrupt irradiance and set-point changes, parametric uncertainty, and dc bus load variations.**

***Index Terms*—DC/DC power converter, input–output linearization (IOL) controller, maximum power point tracking (MPPT) technique, photovoltaic (PV) systems, proportional–integral (PI) control.**

I. Introduction

In recent years, renewable energy sources have been an important research topic around the world. The main objective of renewable energy technologies is to reach a substantial percentage of the global electricity production and, in this way, to mitigate the energy-related emissions of CO_2 delivered to the environment. Among the most promising renewable energy sources is the photovoltaic (PV) solar energy. However, the high initial investment is still the main obstacle that faces this technology. In addition, to maximize the resulting revenue, the optimal operation of the PV modules (PVMs) is required to extract the maximum available energy. In this context, different

Manuscript received May 15, 2014; revised August 5, 2014 and September 7, 2014; accepted October 1, 2014. Date of publication November 11, 2014; date of current version May 8, 2015.

D. R. Espinoza-Trejo and E. Bárcenas-Bárcenas are with the Department of Mechatronics Engineering, Coordinación Académica Región Altiplano, Universidad Autónoma de San Luis Potosí, 78700 San Luis Potosí, México (e-mail: drespinozat@ieee.org; ernesto.barcenas@uaslp.mx).

D. U. Campos-Delgado is with the College of Sciences, Universidad Autónoma de San Luis Potosí, 78290 San Luis Potosí, México (e-mail: ducd@fciencias.uaslp.mx).

C. H. De Angelo is with the Grupo de Electrónica Aplicada, Universidad Nacional de Río Cuarto, X5804BYA Río Cuarto, Argentina, and also with the Consejo Nacional de Investigaciones Científicas y Técnicas, C1033AAJ Buenos Aires, Argentina (e-mail: cdeangelo@ieee.org).

Color versions of one or more of the figures in this paper are available online at http://ieeexplore.ieee.org.

Digital Object Identifier 10.1109/TIE.2014.2369456

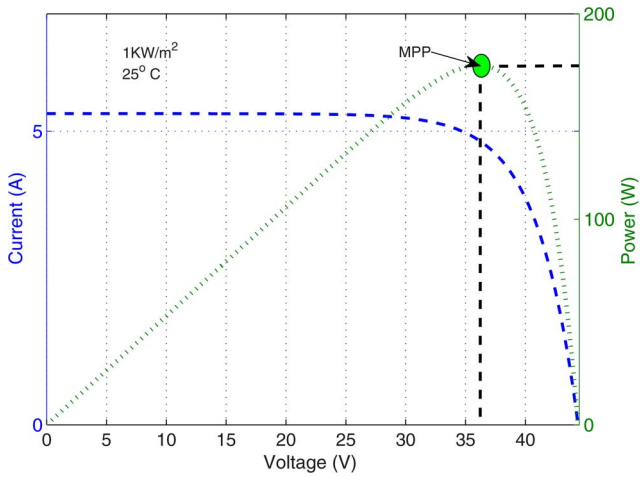

Fig. 1. Characteristic curves. (Blue) I–V curve. (Green) P–V curve.

maximum power point tracking (MPPT) techniques have been proposed in the literature. Under uniform irradiance solar conditions, PVMs exhibit a *power–voltage* curve in which a global maximum, known as *maximum power point* (MPP), can be observed (see Fig. 1) [1]. The purpose of the MPPT techniques is to operate the PVM in the MPP, so as to transfer the maximum power to the load. This condition is possible by adjusting the switching pattern (*duty cycle*) of a dc/dc power converter connected in cascade with the PVM, in order to regulate its voltage or current [2], [3]. Basically, there are two different ways to achieve this operation [4]: 1) direct methods, which are mainly focused on the MPP searching by using (*sensing*) input or output power converter signals and by adjusting directly the duty cycle of the same converter, and 2) searching techniques in conjunction with a closed-loop control strategy as illustrated in Fig. 2. It is worth noting that this paper is focused on the latter philosophy due to the robustness and disturbance rejection capabilities inherited by a feedback scheme, at the price of a more involved system.

Among the MPPT techniques proposed initially in the literature, the ones commonly applied are the following: 1) perturb and observe (P&O) and 2) incremental conductance (IC) [5]. These techniques have been employed both as a direct method or in conjunction with traditional control strategies (*usually a proportional–integral (PI) controller*) [6]. The P&O direct method consists in disturbing the duty cycle of the dc/dc power converter, evaluating if the power in the terminals of the PVM increases or decreases, and then defining an action for the next step of the adjustment law. However, the problem with this

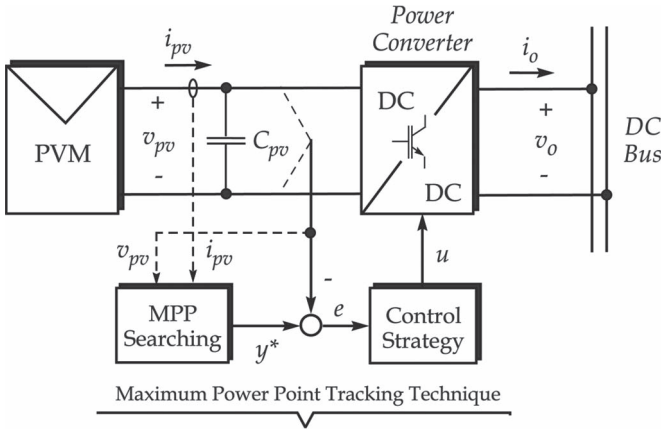

Fig. 2. DC–DC power converter as MPPT system.

method is that the system oscillates around the MPP, and as a consequence, some energy is wasted in this process [7]. An evaluation of the P&O direct method and P&O+PI controller techniques for water pumping systems was recently reported in [8]. Meanwhile, the IC+PI controller method is based on the fact that the first derivative of the power $P_{\rm pv}$ with respect to the steady-state voltage $V_{\rm pv}$ of the PVM is equal to zero in the MPP (see Fig. 1). Taking into account that $P_{\rm pv} = V_{\rm pv} I_{\rm pv}$, then

$$\frac{dP_{\rm pv}}{dV_{\rm pv}} = 0 \;\Rightarrow\; 0 = \frac{I_{\rm pv}}{V_{\rm pv}} + \frac{dI_{\rm pv}}{dV_{\rm pv}} \tag{1}$$

where $I_{\rm pv}$ denotes the steady-state current of the PVM. As a consequence, if the current and voltage from the PV array are available, then an error power signal could be generated, which is compensated by the PI controller [9]. Nonetheless, the authors in [9] did not provide an analytical stability evaluation of the methodology nor a strategy to tune the controller gains. Recently, this classical approach of the PI controller with a novel optimization technique for the control parameters was proposed in [10].

The current PV applications, for example, dc microgrids with battery management capability and sustainable mobility, require a fast dynamic response under sudden irradiation drops and load variations. Hence, novel results that consider the dc/dc power converter dynamics have recently been reported in [2] and [11]–[15], which are mainly focused on achieving a better closed-loop performance than classical approaches. In [11], MPPT was studied like a nonlinear time-varying control problem. Global asymptotic stability of the closed-loop system is guaranteed throughout the existence of a Lyapunov function. The main advantage of this technique is that there is no need to calculate periodically the MPP voltage. However, the derivatives of the reference point with respect to time are required. Thus, this method is limited by the accuracy of the numerical time derivatives and the inherited lack of robustness. On the other hand, in [12], a voltage-oriented Takagi–Sugeno fuzzy controller was proposed by considering parametric uncertainty and partial feedback of the state vector. Nonetheless, the approach results in a complex fuzzy logic controller, where, also, the load current is assumed measurable, which increases the implementation cost.

More recently, small-signal models have been employed for controller design in [13]–[15]. In [13] and [14], the MPPT problem was studied from a current-oriented perspective. In [13], a cascade control structure is proposed by using the sliding-mode control technique with a current-based MPPT approach. The inner loop regulates the current flowing into the capacitor connected at the terminals of the PVM; meanwhile, in the outer loop, the PV voltage is compensated. An advantage of this scheme is that the current-based MPPT cascade control makes up for the intrinsic instability due to irradiation drops [4]. Meanwhile, a sliding-mode controller design, as MPPT technique, was proposed for fourth-order dc/dc power converters in [14]. In fact, a more formal analysis of the previous results presented in [13] was given in [14]. On the other hand, voltage- and current-oriented digital predictive controllers were proposed in [2]. Once again, a cascade control structure was suggested to compensate for abrupt irradiance variations. According to this study, the best performance is obtained when the inductor current is employed in the inner loop, whereas a voltage outer loop is selected. Newly, a two-level adaptive controller was proposed in [15] in order to assign the dynamic characteristics of the power conversion strategy as a damped system. In this case, a ripple correlation control technique is used for calculating the duty cycle that delivers the maximum power to the load in steady state. Meanwhile, a model reference adaptive control is used in the second level. Thus, departing from [15] and the previous efforts in the field, the critical issues to be considered in the new MPPT algorithms include system complexity, robustness to parameter uncertainty, and dynamical performance. Finally, the major characteristics of all the MPPT techniques revised in this paper are summarized in Table I.

In this context, the technical contributions of the MPPT control strategy proposed in this paper are described next.

1) The MPPT technique is based on an input–output linearization (IOL) control strategy [16]. The well-known drawback of this control strategy is the necessity of an exact cancellation of the nonlinear dynamics in order to obtain a good performance. For this purpose, only two assumptions have been considered to obtain a robust control system, namely: A1) The voltage reference is assumed constant or slowly time varying (i.e., its time derivative is zero), and A2) the dc/dc converter is operating in a continuous-conduction mode. Furthermore, no assumptions about climate conditions are made, and also, no linearized models around operating points are required.
2) The closed-loop control strategy results in a cascade control structure, where the inductor current is used in the inner loop; meanwhile, in the outer loop, the PV voltage is regulated. This control structure allows to compensate sudden irradiation drops. The proof of asymptotic stability and a criterion for tuning the controller gains are detailed in this paper.
3) The load of the dc/dc converter is not required to be a resistor or a constant voltage source, as it has been considered in several works previously reported in the literature [2], [15]. Here, a sector condition for the load current is only assumed in order to satisfy internal stability and rejection of load variations. This sector condition is guaranteed in most of the current PV applications, for example, dc microgrids with battery management

TABLE I
COMPARATIVE TABLE OF MPPT+CONTROL TECHNIQUES REPORTED IN THE LITERATURE ($v_{\rm pv}$ AND $i_{\rm pv}$ DENOTE THE INSTANTANEOUS VOLTAGE AND CURRENT IN THE PVM, RESPECTIVELY, i_L IS THE CURRENT FROM THE INDUCTOR IN THE DC/DC CONVERTER, $i_{C_{\rm pv}}$ IS THE CURRENT FROM THE CAPACITIVE FILTER $C_{\rm pv}$ IN THE PVM, v_o AND i_o ARE THE OUTPUT VOLTAGE AND CURRENT IN THE SAME CONVERTER, AND v_{cs} IS THE VOLTAGE IN THE CAPACITOR OF THE OUTPUT LC FILTER IN THE DC/DC CONVERTER)

Reference	Number of Sensors[1]	Load Type[2]	DC/DC Converter	Model Used for Control Design	Control Strategy	MPP Searching Technique	Validation Strategy	Evaluation Against Parametric Uncertainty	Rejection to Low Frequency Oscillations in the DC Bus Load
[2]	4 $(v_{pv}, i_{pv}, i_L, v_o)$	Resistive Load	BOOST	System State Equations	Predictive Digital Control	P&O	Experimental	No	No
[10]	3 (v_{pv}, i_{pv}, v_o)	Grid Connected Inverter	SEPIC	-	Optimised PID Control	P&O	Simulation & Experimental	No	No
[11]	3 (i_L, v_o, i_o)	Resistive Load	BUCK	Averaged Model	Nonlinear Time-Varying Dynamic Feedback Controller	-	Simulation	Yes	No
[12]	4 $(v_{pv}, i_{pv}, i_L, i_o)$	Resistive Load	BUCK	Nonlinear Averaged Model	Takagi-Sugeno Fuzzy Controller	IC	Simulation & Experimental	Yes	No
[13]	3 $(v_{pv}, i_{pv}, i_{Cpv})$	Battery	BOOST	Small-Signal Model	Sliding Mode Control	P&O	Simulation & Experimental	No	Yes
[14]	4 $(v_{pv}, i_{pv}, i_{Cpv}, v_{cs})$	Battery	SEPIC	Small-Signal Model	Sliding Mode Control	P&O	Simulation & Experimental	Yes	No
[15]	2 (v_{pv}, i_{pv})	Battery	BOOST	Small-Signal Model	Model Reference Adaptive Control (MRAC)	Ripple Correlation Control (RCC)	Simulation	No	No
This work	3 (v_{pv}, i_{pv}, i_L)	Battery	BUCK	Nonlinear Averaged Model	Input-Ouput Linearization Controller	Fractional Method	Experimental	Yes	Yes

[1]The category Number of Sensors in Table I has been evaluated by considering the number of sensors required by the Control Strategy and the MPP Searching Technique. It is worth noting that in this paper the number of sensors is the same even if other MPP searching technique is selected for voltage reference generation purposes.

[2]The category Load Type in Table I reflects the load type employed in the MPPT system evaluation.

capability [17], MPPT-distributed schemes [18], or stand-alone applications [19].

4) Finally, the MPPT controller is experimentally validated under abrupt irradiance drops, load variations, and parametric uncertainty to show its robustness to these perturbations.

II. SYSTEM MODELING

Current PV applications require different dc/dc converter topologies. For example, a study of four different topologies of these converters, as possible options for their cascade connection, was presented in [20]. Advantages and drawbacks of such topologies were analyzed in detail in the same paper. Recently, a buck converter was chosen for dc microgrids [17], distributed MPPT schemes [18], and stand-alone applications [19]. Hence, in this study for the design and implementation of the proposed MPPT controller, the buck converter is considered because of its simplicity and high efficiency [18]. Nonetheless, the same methodology described in this paper can be extrapolated to other dc/dc converters, such as boost, buck/boost, single-ended primary-inductor converter (SEPIC), and Cúk, and it will be reported in future works. In the following, the nonlinear dynamic model of the dc/dc converter employed in the MPPT system is presented in this section.

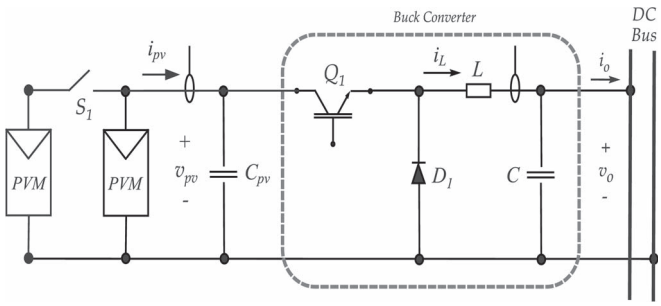

Fig. 3. Buck power converter as MPPT.

A. Power Converter Modeling

The power converter used in this study is presented in Fig. 3. This system is formed by the buck converter and a capacitive filter $C_{\rm pv}$. The average model of the system is represented by the following set of equations:

$$\begin{aligned}\dot{x}_1 &= -\frac{1}{C_{\rm pv}}x_2 u + \frac{1}{C_{\rm pv}}i_{\rm pv}\\ \dot{x}_2 &= -\frac{1}{L}x_3 + \frac{1}{L}x_1 u\\ \dot{x}_3 &= \frac{1}{C}x_2 - \frac{1}{C}i_o.\end{aligned} \tag{2}$$

The state vector is defined by $\mathbf{x} = (x_1, x_2, x_3)^T = (v_{\rm pv}, i_L, v_o)^T$, where $v_{\rm pv}$ represents the input voltage in the terminals of the capacitor $C_{\rm pv}$, i_L is the current of inductor L, and v_o is the voltage in the terminals of the output capacitor C. The PV current $i_{\rm pv}$ is generated by the PVM. The signal u is the control variable that represents the duty cycle for the switch Q_1, and consequently, it has a limited operating range, $u \in [0, 1]$. Finally, in this model, an arbitrary load has been considered, which is characterized by its electrical properties $(v_o, i_o) = (x_3, g(x_3))$. In this case, a sector condition for the function $g(\cdot)$ is only necessary in order to satisfy internal stability and to reject load variations, as described in detail through Proposition 1. Note that the mathematical model shown in (2) presents nonlinear dynamics. Hence, conventional linear control techniques might result in a poor MPPT performance. Therefore, in Section III, an IOL technique with integral action in the tracking error, plus a feedforward action on $i_{\rm pv}$, is proposed to achieve the desired performance under sudden irradiation drops, set-point changes, and load disturbances.

III. Proposed MPPT Controller

In this section, the proposed MPPT control strategy is derived based on the model of the dc/dc converter in (2) and an IOL technique [16]. Moreover, the proof of stability of the resulting zero dynamics, as one of the main results in this paper, is studied in detail in this section. Finally, a strategy to generate the voltage reference for the control law is also described.

Even though references about IOL control have been presented in the literature of power electronics [21], [22], only one reference about the implementation of an IOL controller for MPPT applications has been described so far [23]. In that work, a boost converter was employed with a current-oriented control perspective for MPPT applications, where the control law is dependent on the parameters of the PV array and power circuit, in contrast to the proposal in this paper.

A. Input–Output Linearizing State Feedback Control

To address the MPPT challenges outlined in Section I, the voltage of the PVM is chosen as output $y = x_1$. The first derivative of the output is given by

$$\dot{y} = -\frac{1}{C_{\rm pv}} x_2 u + \frac{1}{C_{\rm pv}} i_{\rm pv}. \tag{3}$$

Since the control signal u appears in the first derivative, this means that the nonlinear system presents a relative degree $\rho = 1$ in $\mathbb{R}^3$. As a consequence, two internal states are unobservable by the control action [16]. However, in the following, internal stability is guaranteed for several load scenarios. Next, assuming that the state x_2 is available for feedback, a linearizing control law is defined as

$$u = -\frac{1}{x_2} \cdot \sigma \tag{4}$$

where σ is an auxiliary control law. Observe that the elements of the buck converter and its switching frequency must be selected to guarantee a continuous-conduction mode such that $x_2 > 0$ for all time, and in this way, the control law (4) is well defined. Thus, by substituting the control signal (4) in the first derivative (3), the following result is obtained:

$$C_{\rm pv}\dot{y} = \sigma + i_{\rm pv}. \tag{5}$$

To provide robustness to the MPPT strategy, the auxiliary signal σ is constructed by a PI action with respect to the reference error in the PVM voltage, plus a feedforward term that cancels the input current $i_{\rm pv}$

$$\sigma = C_{\rm pv}\dot{y}^\star + K_p(y^\star - y) + K_i \int (y^\star - y)dt - i_{\rm pv} \tag{6}$$

where $y^\star$ denotes the voltage reference. As a result, $y^\star$ will be chosen to guarantee the MPP in the PVM. By substituting (6) in (5), the tracking error dynamics are obtained (see Section III-C)

$$\ddot{e} + \frac{K_p}{C_{\rm pv}}\dot{e} + \frac{K_i}{C_{\rm pv}} e = 0 \tag{7}$$

where $e = y^\star - y$. Note that (7) satisfies the following characteristic equation:

$$\lambda^2 + \frac{K_p}{C_{\rm pv}}\lambda + \frac{K_i}{C_{\rm pv}} = 0. \tag{8}$$

In this way, to guarantee the asymptotic convergence to the voltage reference $y \to y^\star$, the error dynamics in (7) are assigned to the standard second-order system

$$\lambda^2 + 2\xi\omega_n\lambda + \omega_n^2 = 0 \tag{9}$$

where ξ represents the damping factor and ω_n is the undamped natural frequency. Therefore, to ensure asymptotic stability, it is enough to choose two positive gains K_p and K_i that achieve the desired transient response. Nevertheless, K_p and K_i have been defined such that the step response of the system behaves like a slightly underdamped system, in order to remove transient oscillations in the PVM voltage (x_1) due to changing environmental conditions. For this purpose, the damping factor is chosen as $\xi = (1/\sqrt{2})$, and the settling time (t_s) is considered equal to $t_s = 10T_{sw}$, where T_{sw} is the switching period [2], [13]. Thus, the PI controller's gains are chosen as

$$K_p = \frac{4}{5} C_{\rm pv} f_{sw};\ K_i = \frac{8}{25} C_{\rm pv} f_{sw}^2 \tag{10}$$

where $f_{sw} = 1/T_{sw}$ represents the switching frequency. Now, by taking into account the voltage reference generation stage described in the Section III-C, for the controller implementation, it is assumed that the voltage reference is constant or slowly time varying, i.e., $\dot{y}^\star \approx 0$. In this way, from (6), the following auxiliary control law σ is considered in the experimental evaluation:

$$\sigma = K_p(y^\star - y) + K_i \int (y^\star - y)dt - i_{\rm pv}. \tag{11}$$

Hence, departing from (4) and (11), the resulting control algorithm does not depend on the parameters of the dc/dc converter nor PV array parameters. Only K_p and K_i are determined as functions of the capacitor $C_{\rm pv}$ and frequency f_{sw}. Nonetheless, during the implementation, only $C_{\rm pv}$ could have a parametric

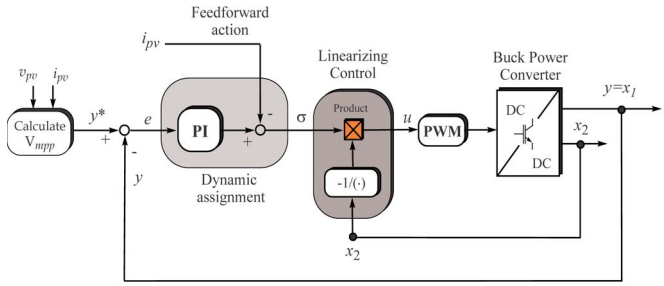

Fig. 4. Proposed MPPT control strategy.

variation since f_{sw} is fixed. To evaluate the robustness, in the experimental results section, the effect on the closed-loop dynamic response under parametric uncertainty of the capacitor $C_{\rm pv}$ is illustrated for all the experiments. Thus, by using (4) and (11), a voltage-oriented controller insensitive to parametric uncertainty is obtained by this control strategy. A block diagram of this control strategy is presented in Fig. 4. As can be observed, the MPPT model-based technique proposed in this paper is posed like a cascade control structure [2], with a PI action on the tracking error e, plus a feedforward action on the PV current $i_{\rm pv}$, which makes the MPPT control strategy useful for several applications for which abrupt irradiance variations are common [13]. Hence, the robustness to model parameters and dc bus voltage variations is achieved at the price of three measurements for control: PVM voltage and current $(v_{\rm pv}, i_{\rm pv})$ and inductor current i_L. In addition, the MPPT is also independent from the rating power of the dc/dc converter that mainly depends on the semiconductor and passive element sizing and heat dissipation capabilities but not on the control philosophy. Finally, the MPPT control technique proposed in this paper is able to transfer the maximum energy to an unknown load by ensuring internal stability, as described in the following section.

B. Zero Dynamics

In this section, one of the main contributions of this paper is described, where the load of the dc/dc converter is extended further from a simple resistor or constant voltage source. In this way, an unknown load is considered. Nevertheless, internal stability for the unobservable dynamics is guaranteed for several load conditions. With this aim, in order to characterize the zero dynamics, the state vector $\mathbf{x}$ is restricted to

$$\mathbf{Z} = \left\{\mathbf{x} \in \mathbb{R}^3 | x_1 = 0\right\} \tag{12}$$

with $u = 0$, which leads to the following autonomous system for the dc/dc converter model in (2):

$$\begin{aligned} \dot{x}_2 &= -\frac{1}{L}x_3 \\ \dot{x}_3 &= \frac{1}{C}x_2 - \frac{1}{C}i_o. \end{aligned} \tag{13}$$

By assuming that the load current i_o is a function of the state x_3, i.e., $i_o = g(x_3)$, then, the zero dynamics given by

$$\eta : \begin{cases} \dot{x}_2 = -\frac{1}{L}x_3 \\ \dot{x}_3 = \frac{1}{C}x_2 - \frac{1}{C}g(x_3) \end{cases}$$

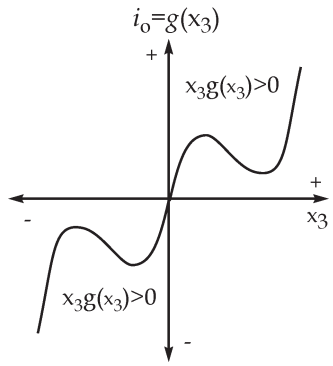

Fig. 5. Sector condition for the load current $i_o = g(x_3)$.

are a minimum phase system, as described in the following proposition. This result guarantees that the state variables x_2 and x_3 are bounded in spite of dc bus voltage variations; meanwhile, the state variable x_1 follows asymptotically its voltage reference.

Proposition 1: The dynamical system η has the origin as a unique and asymptotically stable equilibrium point if

$$g(0) = 0;\ x_3 g(x_3) < 0;\ \forall\, x_3 \in (-\infty, 0) \cup (0, \infty). \tag{14}$$

■

Proof of Proposition: First, by the property in (14), $(0, 0)$ is the only equilibrium point of η, and the following quadratic energy function is proposed:

$$V(x_2, x_3) = \frac{1}{2}Lx_2^2 + \frac{1}{2}Cx_3^2. \tag{15}$$

By taking its derivative along the trajectories of the system and by using the dynamic equations of η, it is obtained that

$$\dot{V}(x_2, x_3) = -x_3 g(x_3) < 0. \tag{16}$$

Hence, the time derivative $\dot{V}$ is negative definite $\forall\, x_3 \neq 0$ but independent of x_2. However, by LaSalle's theorem [16], it can be concluded that the dynamical system η has an asymptotically stable equilibrium point (0, 0) because

$$x_3 = 0 \ \Rightarrow\ x_2 = 0.$$

Therefore, the system η is a minimum phase. ■

Note that the assumption required for the load current i_o is satisfied when the MPPT system acts as a power source, i.e., the PVM energy is always being injected to the dc load bus, even if the dc bus presents variations, as can be observed from Fig. 5, which implies the robustness to oscillations in the dc voltage bus [13] or noise signals.

C. Voltage Reference Generation

Finally, to obtain the reference voltage $y^\star$, different techniques can be considered [6], [24]–[27]. Recently, some techniques to mitigate the effects of partial shading are described in [24], [28]–[30]. However, even if it could be possible to identify the global MPP, each module cannot be operated at its own MPP [31]. Hence, distributed MPPT schemes are being proposed as solutions to partial shading and mismatching conditions [4], where the buck converter is suitable for series connection. However, the contribution of this paper is not

directed toward a method to calculate the MPP. In fact, the control algorithm proposed in this study is independent from the technique used to calculate the MPP. Hence, the simplest technique to calculate the voltage associated to the MPP is known as *fractional method* [6]. This technique is adopted here for its simplicity, which is based on the fact that the MPP voltage is a percentage of the open-circuit voltage $V_{\rm oc}$, i.e.,

$$y^{\star} \approx 0.8\, V_{\rm oc}. \tag{17}$$

Finally, note that the open-circuit voltage is periodically updated in our implementation and maintained as a constant value after each measurement.

IV. Experimental Evaluation

In this section, an experimental evaluation of the voltage-oriented IOL controller for MPPT in PV systems is carried out. The technical contributions of this paper are highlighted through the experimental tests. The following scenarios are considered.

T1: The performance of the proposed MPPT strategy is evaluated under set-point changes and parametric uncertainty of $\pm 10\%$ on the input capacitance value $C_{\rm pv}$.

T2: The performance of the proposed MPPT strategy is evaluated under sudden irradiance drops and parametric uncertainty of $\pm 10\%$ on the input capacitance value $C_{\rm pv}$.

T3: The MPPT operation, internal stability, and disturbance rejection in the PV voltage terminals are evaluated in spite of low frequency disturbances present in the dc voltage bus acting as load for the dc/dc converter.

A. Test Bench

To validate the ideas presented in this paper, the experimental evaluations are carried out in a test bench with a nominal PV power of 350 W. In Fig. 6(a), the experimental PV array is illustrated. Nonetheless, only one of these PVMs has been used in the experimental evaluation. This condition is selected because the distributed MPPT schemes are currently considered to mitigate the effects of partial shading. The PVM parameters are defined in Table II, where V_m and I_m denote the voltage and current at the MPP under standard test conditions (STCs), I_{sc} is the short-circuit current in STC, $V_{\rm oc}$ is the open-circuit voltage in STC, and α and β are the current and voltage temperature coefficients, respectively. For the dc/dc power converter, a buck topology is employed in this work (see Fig. 3), which is operating at a switching frequency of 15 kHz. The experimental prototype is shown in Fig. 6(b), where the capacitor $C_{\rm pv}$ is located at the input terminals of the dc/dc converter such that the PV input voltage measurement is not influenced by the cable path from the PVM. The control algorithm is implemented in a DS1104 dSpace board at a sampling frequency of 60 kHz. It should be noted that the PWM technique was implemented outside the dSpace board with analog electronic circuits. For performance visualization, the data acquisition of the closed-loop signals was first carried out in the dSpace board and then exported to Matlab for plotting. The parameters of the power converter are $C_{\rm pv} = 300\ \mu$F, $L = 180\ \mu$H, and $C = 500\ \mu$F, which were selected in order to guarantee a continuous-conduction mode and a minimal output power of 9 W. Also, in the experimental results, a 12-V battery was selected as a load, with a capacity of 80 Ah. The power diode D_1 and the power switch Q_1 are STTH30R04W and IRFP250N, respectively. Two LA55-P current transducers (LEM) were employed for the measurements of the PVM and inductor currents $(i_{\rm pv}, i_L)$.

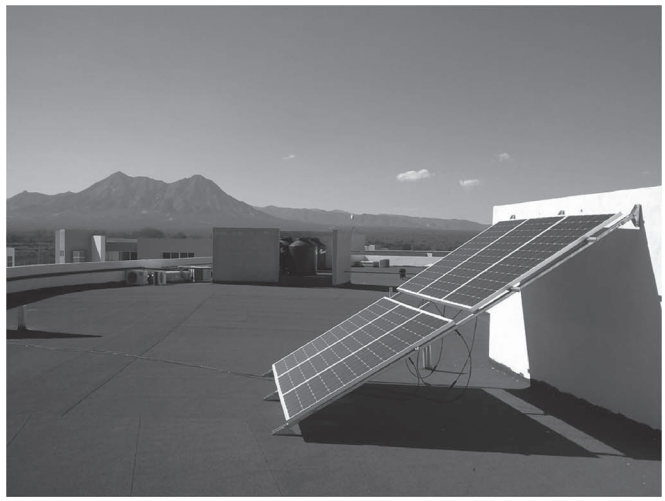

(a)

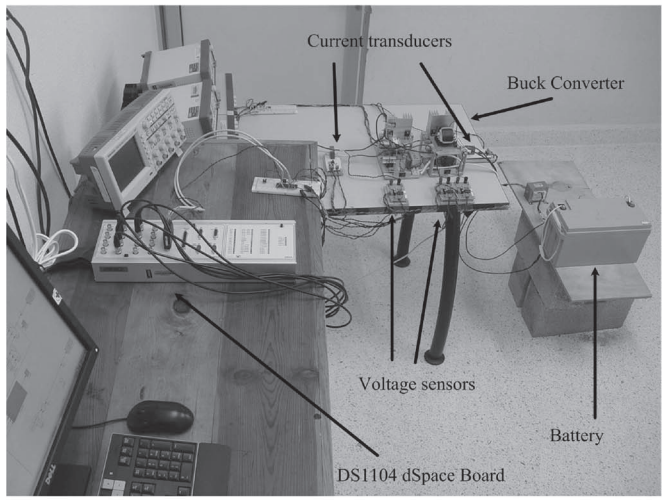

(b)

Fig. 6. Test bench with a nominal PV power of 350 W. (a) PVMs employed in the experimental results. (b) Experimental prototype of the dc/dc power converter.

TABLE II
Set of Parameters of the PVM

Parameter	Value	Parameter	Value
V_m	35.2 V	I_m	4.95 A
V_{oc}	44.2 V	I_{sc}	5.2 A
α	1.2mA/C$^{\circ}$	β	-0.157V/C$^{\circ}$

B. Experimental Test T1

In this test, the reference tracking performance is evaluated by a set-point update due to a change in the MPP. Moreover, since the parameter $C_{\rm pv}$ is a key factor for the PI controller gain selection, the results for $\pm 10\%$ parametric uncertainty in the nominal value of $C_{\rm pv}$ are also evaluated in these experiments.

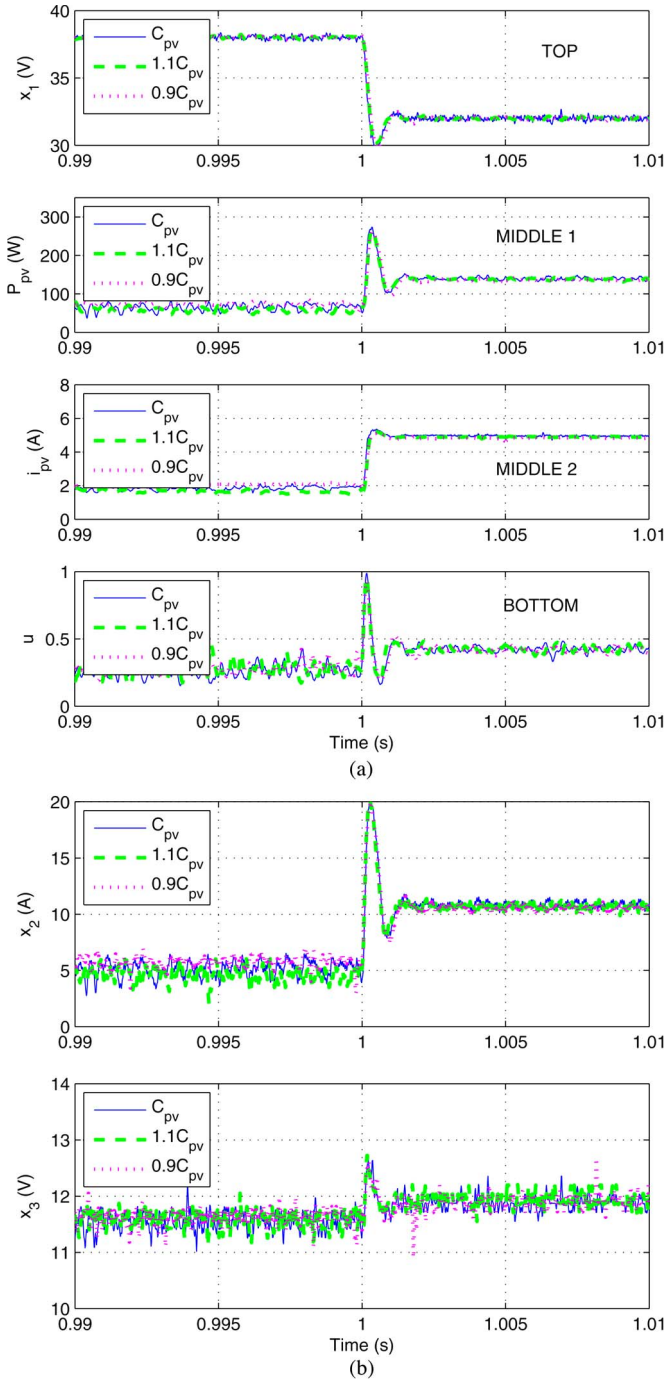

Fig. 7. Experimental test T_1 for a set-point change with parametric uncertainty of $\pm 10\%$ on the capacitance value $C_{\rm pv}$. (a) Top: Voltage in terminals of capacitor $C_{\rm pv}$; middle 1: PV power $P_{\rm pv}$; middle 2: PV current; Bottom: duty cycle u. (b) Top: Inductor current $x_2 = i_L$; Bottom: output voltage $x_3 = v_o$.

As can be seen in Fig. 7, at $t = 1.0$ s, there is a set-point change from 38 to 32 V. The closed-loop dynamics are assigned through the PI controller gains, which were selected to deliver a slightly underdamped step response. The PI controller parameters are $K_p = 3.6$ and $K_i = 21\,600$. For this case, the closed-loop settling time is chosen as $t_s = 0.66$ ms. As illustrated in the top plot of Fig. 7(a), in all cases, the PV voltage is well regulated in both voltage references in spite of parametric uncertainty. Also, as a consequence of the set-point change, an

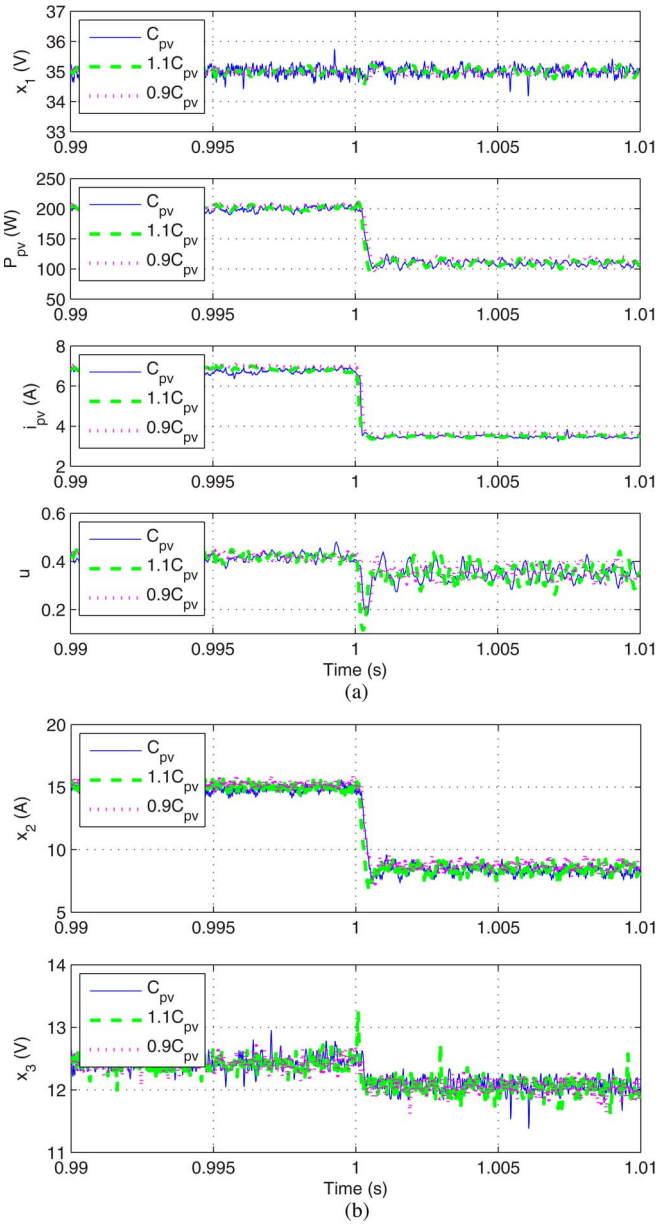

Fig. 8. Experimental test T_2 for a sudden irradiance drop of approximately 50% with parametric uncertainty of $\pm 10\%$ on the capacitance value $C_{\rm pv}$. (a) Top: Voltage in terminals of capacitor $C_{\rm pv}$; middle 1: PV power $P_{\rm pv}$; middle 2: PV current; bottom: duty cycle u. (b) Top: Inductor current $x_2 = i_L$; bottom: output voltage $x_3 = v_o$.

increment from 60 to 140 W in the PV power $P_{\rm pv} = v_{\rm pv} i_{\rm pv}$ is obtained, [see middle 1 plot of Fig. 7(a)], as well as an increment in the PVM current [see middle 2 plot of Fig. 7(a)], while the duty cycle is adjusted to compensate this condition [see bottom plot of Fig. 7(a)]. Meanwhile, the internal dynamics are shown in the two plots of Fig. 7(b). The output voltage x_3 is kept around the operating voltage of the battery, and the inductor current x_2 also presents a bounded operation. In this way, internal stability and MPPT operation are observed in these scenarios, as described by Proposition 1.

C. Experimental Test T2

In these experiments, an abrupt irradiance drop of approximately 50% is considered. Such a condition is obtained by

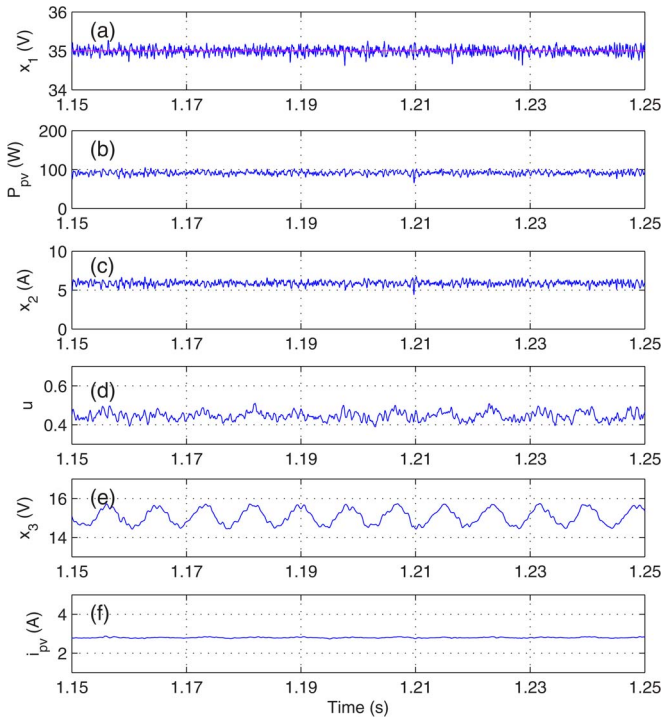

Fig. 9. Closed-loop response for experimental test T_3 under load variations of low frequency: (a) Voltage in terminals of capacitor $C_{\rm pv}$, (b) PV power $P_{\rm pv}$, (c) inductor current i_L, (d) duty cycle u, (e) output voltage in the terminals of capacitor C, and (f) PV current.

disconnecting two panels in the parallel connection through switch S_1, as illustrated in Fig. 3 [2]. Again, $\pm 10\%$ of the parametric uncertainty in the nominal capacitance value $C_{\rm pv}$ is also taken into account during the experiments. Also, the same PI controller parameters have been chosen. As can be seen in the middle 1 plot of Fig. 8(a), at $t = 1.0$ s, there is a sudden irradiance drop from 200 to 100 W in 400 μs, while the PVM voltage is regulated at the MPP, i.e., $y^\star = 0.8 \times V_{\rm oc} = 35$ V (see Table II). This abrupt change can be also seen in the PV current as shown in the middle 2 plot of Fig. 8(a), while the duty cycle is adjusted to compensate this condition [see the bottom plot of Fig. 8(a)]. Hence, any underdamped responses in the PVM voltage due to rapid changes in solar irradiance have been completely removed. Moreover, once more, the internal dynamics have been kept bounded, as shown in the two plots of Fig. 8(b). Again, the output voltage x_3 is kept around the operating voltage of the battery, and the inductor current is updated to this new condition. Thus, internal stability and MPPT operation are also observed even under these harsh conditions, as was expected departing from Proposition 1.

D. Experimental Test T3

Finally, the rejection of low frequency voltage variations located into the buck converter output is illustrated through this experiment. In this way, the PVM voltage is kept in its voltage reference, $y^\star = 35$ V. Once more, the ability of rejecting sinusoidal disturbances at different frequencies affecting the buck converter output is guaranteed by Proposition 1. Because of that, the noise rejection capability is also satisfied by the technique proposed in this paper. In this test, the low frequency oscillation is intentionally induced with a transformer plus a function generator in series with the lead–acid battery acting as a load. The disturbance is a sinusoidal signal with a frequency of 120 Hz and an amplitude of 1 V peak to peak [see Fig. 9(e)]. As can be seen in Fig. 9(a), the PVM voltage is regulated at 35 V in spite of the disturbance acting on the dc bus output voltage. Thus, the PV power is kept in its maximum operating point of 100 W all the time [see Fig. 9(b)]. As was expected, the duty cycle is adjusted to compensate the low frequency voltage variations, which can be observed from Fig. 9(d). Finally, note that the state variables x_2 and x_3 are bounded [see Fig. 9(c) and (e)] as expected by the result in Proposition 1.

V. Final Remarks and Future Work

In this paper, a simple and robust MPPT model-based strategy has been proposed. The control strategy is based on an IOL controller, which establishes a linear mapping between the duty cycle and the PVM voltage. The resulting MPPT controller has a cascade structure with two feedback loops, which is able to compensate sudden irradiance drops. Only the states x_1 (*voltage in the terminals of the input capacitor* $C_{\rm pv}$) and x_2 (*inductor current*) from the buck converter were assumed measurable, plus the PV current $i_{\rm pv}$ which acts as a feedforward term. By assuming a sector condition for the load current i_o, it was possible to demonstrate that the zero dynamics have an asymptotically stable equilibrium point. In turn, this condition implies the robustness against oscillations in the dc voltage bus. The experimental results were able to highlight the desired closed-loop performance under abrupt irradiance and set-point changes, parametric uncertainty, and disturbances rejection on the PVM voltage terminals. Finally, this methodology can be extrapolated to other dc/dc converters, and it will be reported in future works.

References

[1] Y. Mahmoud, W. Xiao, and H. H. Zeineldin, "A simple approach to modeling and simulation of photovoltaic modules," *IEEE Trans. Sustain. Energy*, vol. 3, no. 1, pp. 185–186, Jan. 2012.
[2] P. E. Kakosimos, A. G. Kladas, and S. N. Manias, "Fast photovoltaic-system voltage or current-oriented MPPT employing a predictive digital current-controlled converter," *IEEE Trans. Ind. Electron.*, vol. 60, no. 12, pp. 5673–5685, Dec. 2013.
[3] P. P. Dash and M. Kazerani, "Dynamic modeling and performance analysis of a grid-connected current-source inverter-based photovoltaic system," *IEEE Trans. Sustain. Energy*, vol. 2, no. 4, pp. 443–450, Oct. 2011.
[4] E. Romero-Cadaval *et al.*, "Grid-connected photovoltaic generation plants," *IEEE Ind. Electron. Mag.*, vol. 7, no. 3, pp. 6–20, Sep. 2013.
[5] D. Sera, L. Mathe, T. Kerekes, S. V. Spataru, and R. Teodorescu, "On the perturb and observe and incremental conductance MPPT methods for PV systems," *IEEE J. Photovolt.*, vol. 3, no. 3, pp. 1070–1078, Jul. 2013.
[6] M. A. Gomes de Brito, L. Galotto, Jr., L. P. Sampaio, G. de Azevedo e Melo, and C. A. Canesin, "Evaluation of the main MPPT techniques for photovoltaic applications," *IEEE Trans. Ind. Electron.*, vol. 60, no. 3, pp. 1156–1167, Mar. 2013.
[7] N. Femia, G. Petrone, G. Spagnuolo, and M. Vitelli, "Optimization of perturb and observe maximum power point tracking method," *IEEE Trans. Power Electron.*, vol. 20, no. 4, pp. 963–973, Jul. 2005.
[8] M. A. Elgendy, B. Zahawi, and D. J. Atkinson, "Assessment of perturb and observe MPPT algorithm implementation techniques for PV pumping applications," *IEEE Trans. Sustain. Energy*, vol. 3, no. 1, pp. 21–33, Jan. 2012.
[9] E. Koutroulis, K. Kalaitzakis, and N. C. Voulgaris, "Development of a microcontroller-based photovoltaic maximum power point tracking control system," *IEEE Trans. Power Electron.*, vol. 16, no. 1, pp. 46–54, Jan. 2001.

[10] A. E. Khateb, N. A. Rahim, J. Selvaraj, and M. N. Uddin, "Maximum power point tracking of single-ended primary-inductor converter employing a novel optimisation technique for proportional-integral-derivative controller," *IET Power Electron.*, vol. 6, no. 6, pp. 1111–1121, Jul. 2013.
[11] E. V. Solodovnik, S. Liu, and R. A. Dougal, "Power controller design for maximum power tracking in solar installations," *IEEE Trans. Power Electron.*, vol. 19, no. 5, pp. 1295–1304, Sep. 2004.
[12] C. S. Chiu and Y. L. Ouyang, "Robust maximum power tracking control of uncertain photovoltaic systems: A unified t-s fuzzy model-based approach," *IEEE Trans. Control Syst. Technol.*, vol. 19, no. 6, pp. 1516–1526, Nov. 2011.
[13] E. Bianconi *et al.*, "A fast current-based MPPT technique employing sliding mode control," *IEEE Trans. Ind. Electron.*, vol. 60, no. 3, pp. 1168–1178, Mar. 2013.
[14] E. Mamarelis, G. Petrone, and G. Spagnuolo, "Design of a sliding-mode-controlled SEPIC for PV MPPT applications," *IEEE Trans. Ind. Electron.*, vol. 61, no. 7, pp. 3387–3398, Jul. 2014.
[15] R. Khanna, Q. Zhang, W. E. Stanchina, G. F. Reed, and Z. H. Mao, "Maximum power point tracking using model reference adaptive control," *IEEE Trans. Power Electron.*, vol. 29, no. 3, pp. 1490–1499, Mar. 2014.
[16] H. K. Khalil, *Nonlinear Systems*, 3rd ed. Upper Saddle River, NJ, USA: Prentice-Hall, 2002.
[17] T. Dragicevic, J. M. Guerrero, J. C. Vasques, and D. Skrlec, "Supervisory control of an adaptive-droop regulated dc microgrid with battery management capability," *IEEE Trans. Power Electron.*, vol. 29, no. 2, pp. 695–706, Feb. 2014.
[18] F. Wang *et al.*, "Analysis of unified output MPPT control in subpanel PV converter system," *IEEE Trans. Power Electron.*, vol. 29, no. 3, pp. 1275–1284, Mar. 2014.
[19] A. S. Satpathy, N. K. Kishore, D. Kastha, and N. C. Sahoo, "Control scheme for a stand-alone wind energy conversion system," *IEEE Trans. Energy Convers.*, vol. 29, no. 2, pp. 418–425, Jun. 2014.
[20] G. R. Walker and P. C. Sernia, "Cascade dc-dc converter connection of photovoltaic modules," *IEEE Trans. Power Electron.*, vol. 19, no. 4, pp. 1130–1139, Jul. 2004.
[21] A. Bidram, A. Davoudi, F. L. Lewis, and J. M. Guerrero, "Distributed cooperative secondary control of microgrids using feedback linearization," *IEEE Trans. Power Syst.*, vol. 28, no. 3, pp. 3462–3470, Aug. 2013.
[22] N. Visairo, C. Nunez, J. Lira, and I. Lazaro, "Avoiding a voltage sag detection stage for a single-phase multilevel rectifier by using control theory considering physical limitations of the system," *IEEE Trans. Power Electron.*, vol. 28, no. 11, pp. 5244–5251, Nov. 2013.
[23] D. Mezghani and A. Mami, "Input-output linearizing control of pumping photovoltaic system: Tests and measurements by micro-controller Stm32," *Int. J. Adv. Eng. Technol.*, vol. 4, no. 2, pp. 25–37, Sep. 2012.
[24] A. Bidram, A. Davoudi, and R. S. Balog, "Control and circuit techniques to mitigate partial shading effects in photovoltaic arrays," *IEEE J. Photovolt.*, vol. 2, no. 4, pp. 532–546, Oct. 2012.
[25] T. Esram and P. L. Chapman, "Comparison of photovoltaic array maximum power point tracking techniques," *IEEE Trans. Energy Convers.*, vol. 22, no. 2, pp. 439–449, Jun. 2007.
[26] C. Rodriguez and G. A. J. Amaratunga, "Analytic solution to the photovoltaic maximum power point problem," *IEEE Trans. Circuits Syst. I, Reg. Papers*, vol. 54, no. 9, pp. 2054–2060, Sep. 2007.
[27] J. S. Christy Mano Raj and A. E. Jeyakumar, "A novel maximum power point tracking technique for photovoltaic module based on power plane analysis of I-V characteristics," *IEEE Trans. Ind. Electron.*, vol. 61, no. 9, pp. 4734–4745, Sep. 2014.
[28] K. Ishaque and Z. Salam, "A deterministic particle swarm optimization maximum power point tracker for photovoltaic system under partial shading condition," *IEEE Trans. Ind. Electron.*, vol. 60, no. 8, pp. 3195–3206, Aug. 2013.
[29] B. N. Alajmi, K. H. Ahmed, S. J. Finney, and B. W. Williams, "A maximum power point tracking technique for partially shaded photovoltaic systems in microgrids," *IEEE Trans. Ind. Electron.*, vol. 60, no. 4, pp. 1596–1606, Apr. 2013.
[30] K. S. Tey and S. Mekhilef, "Modified incremental conductance algorithm for photovoltaic system under partial shading conditions and load variation," *IEEE Trans. Ind. Electron.*, vol. 61, no. 10, pp. 5384–5392, Oct. 2014.
[31] M. Miyatake, M. Veerachary, F. Toriumi, N. Fujji, and H. Ko, "Maximum power point tracking of multiple arrays: A PSO approach," *IEEE Trans. Aerosp. Electron. Syst.*, vol. 47, no. 1, pp. 367–380, Jan. 2011.

Diego R. Espinoza-Trejo (A'10) was born in San Luis Potosí, México. He received the B.S. degree in electronics engineering and the M.Sc. and Ph.D. degrees in electrical engineering from the Universidad Autónoma de San Luis Potosí, San Luis Potosí, in 2001, 2004, and 2008, respectively.

In 2009, he joined the Mechatronics Department, Coordinación Académica Región Altiplano, Universidad Autónoma de San Luis Potosí. He is currently a Professor at the Universidad Autónoma de San Luis Potosí and a Researcher at the Consejo Nacional de Ciencia y Tecnología, México. His main research interests include active fault-tolerant control of power electronic systems, wind and photovoltaic systems, fault diagnosis of electric machines, and power quality solutions.

Ernesto Bárcenas-Bárcenas (S'10–M'10) was born in San Luis Potosí, México. He received the B.S. degree in electronics engineering from the Universidad Autónoma de San Luis Potosí, San Luis Potosí, in 2000 and the M.Sc. and Ph.D. degrees in power electronics from the Centro Nacional de Investigación y Desarrollo Tecnológico, Cuernavaca, México, in 2002 and 2008, respectively.

Since 2010, he has been with the Coordinación Académica Región Altiplano of the Universidad Autónoma de San Luis Potosí. His main research interests include power electronics for renewable energy applications, ac–dc conversion, and electric machine drives.

Dr. Bárcenas is a member of the IEEE Power Electronics Society.

Daniel U. Campos-Delgado (S'97–M'02–SM'13) received the B.S. degree in electronics engineering from the Autonomous University of San Luis Potosi, San Luis Potosí, Mexico, in 1996 and the M.S.E.E. and Ph.D. degrees from Louisiana State University, Baton Rouge, LA, USA, in 1999 and 2001, respectively.

In 2001, he joined the College of Sciences of the Autonomous University of San Luis Potosi as a Professor. He has published more than 130 refereed papers in scientific journals and conference proceedings. His research interests include power allocation and pre-equalization in wireless systems, optimization, dynamic modeling, and optimal signal processing.

Dr. Campos-Delgado is currently a member of the Mexican Academy of Sciences. In May 2001, the College of Engineering of Louisiana State University granted him the Exemplary Dissertation Award, and in 2009 and 2013, he received awards as a young researcher from the Autonomous University of San Luis Potosi and the Mexican Academy of Sciences.

Cristian H. De Angelo (S'96–M'05–SM'10) received the Electrical Engineer degree from the Universidad Nacional de Río Cuarto, Río Cuarto, Argentina, in 1999 and the Doctor of Engineering degree from the Universidad Nacional de La Plata, La Plata, Argentina in 2004.

In 1994, he joined the Grupo de Electrónica Aplicada, Universidad Nacional de Río Cuarto. He is currently an Associate Professor at the Universidad Nacional de Río Cuarto and an Independent Researcher with the Consejo Nacional de Investigaciones Científicas y Técnicas, Buenos Aires, Argentina. His research interests include electric and hybrid vehicles, fault diagnosis of electric machines, electric motor control, and renewable-energy generation.